



# Palladium-niobium bimetallic doped organosilica membranes for H<sub>2</sub>/CO<sub>2</sub> separation

Hengfei Zhang, Yibin Wei, Hong Qi\*

State Key Laboratory of Material-Oriented Chemical Engineering, Membrane Science and Technology Research Center, Nanjing Tech University, Nanjing, 210009, China

## ARTICLE INFO

### Keywords:

Bimetallic doping  
Organosilica membrane  
Palladium  
Niobium  
Gas separation

## ABSTRACT

In this work, high-performance palladium-niobium doped 1,2-bis(triethoxysilyl)ethane (Pd-Nb-BTESE) membranes were prepared for H<sub>2</sub>/CO<sub>2</sub> separation by using the sol-gel method. Nb was first incorporated into the organosilica networks in the form of Nb–O–Si covalent bonds, while Pd nanoparticles were successfully embedded into the networks with size of 5–10 nm. Based on the synergetic effects of Pd–Nb doping, the as-prepared membranes showed more appropriate structures for H<sub>2</sub>/CO<sub>2</sub> separation. By controlling the same doping amount of Nb and changing Pd doping contents (n (Pd): n (Si) = 0.05–0.4), we found that the Pd–Nb-BTESE membrane with higher Pd doping content showed higher H<sub>2</sub>/CO<sub>2</sub> permselectivity and stronger H<sub>2</sub> adsorption capacity. The H<sub>2</sub>/CO<sub>2</sub> separation performance of all the prepared Pd–Nb-BTESE membranes surpass the upper bound 2008. The membrane with n (Pd): n (Si) of 0.4 showed a superior H<sub>2</sub>/CO<sub>2</sub> permselectivity of 107 and a high H<sub>2</sub> permeance of  $1.12 \times 10^{-7} \text{ mol m}^{-2} \text{ s}^{-1} \cdot \text{Pa}^{-1}$ . Our findings provide novel insights into tailoring and functionalizing organosilica membranes through bimetallic doping for practical applications.

## 1. Introduction

Membrane-based gas separation technology has been considered more advantageous over conventional gas separation methods such as pressure swing adsorption, cryogenic distillation and solvent absorption, due to its low energy consumption, low operating cost and small footprint [1]. Microporous ceramic membranes have attracted much attention in the applications of separating small gas molecules under harsh industrial conditions because of their excellent thermal, mechanical and chemical stability [2]. In recent years, amorphous silica membranes with tunable microstructures have become some of the most important members in the ceramic membrane family owing to their unique permeance and molecular sieving capability for small gases separation [3]. As the first generation of amorphous silica membranes, tetraethoxysilane (TEOS) derived silica membranes have been extensively studied [4,5]. However, it was found by many researchers that the pure silica membranes were unstable under hydrothermal conditions, which limits their practical applications [6,7]. In the past decade, hybrid organosilica membranes with the incorporation of hydrophobic organic groups derived from bridged silsesquioxane have been proven themselves more hydrothermally stable in applications of pervaporation and gas separation [8,9]. Among organosilica membranes, 1,2-bis-

(triethoxysilyl)ethane (BTESE)-derived organosilica membranes with ethylene-bridged networks provide well-defined pore structures, which make them promising for small gases separation under hydrothermal conditions [10].

H<sub>2</sub>/CO<sub>2</sub> separation under varying hydrothermal conditions is crucial for addressing the global challenges associated with energy security (e.g. hydrogen production) and climate change (e.g. pre-combustion carbon capture) [11–13]. Although pure BTESE-derived organosilica membranes usually exhibited acceptable hydrothermal stability and high H<sub>2</sub> permeance in H<sub>2</sub>/CO<sub>2</sub> separation, the permselectivity of pure BTESE-derived membranes were still unsatisfied to meet the requirements for such applications. Metal doping is one of the efficient approaches to improve H<sub>2</sub>/CO<sub>2</sub> permselectivity for silica-based membranes. Most metal (e.g. Al, Nb and Zr) dopants could endow silica-based membranes with denser structures, leading to a significant increase in their H<sub>2</sub>/CO<sub>2</sub> permselectivity [14–16]. For example, ten Hove et al. reported a Zr-doped BTESE membrane with H<sub>2</sub>/CO<sub>2</sub> permselectivity of 16, which was four times as much as that of their pure BTESE membrane [16]. They believed that the improved H<sub>2</sub>/CO<sub>2</sub> permselectivity was ascribed to the formed denser structure caused by Zr doping.

Moreover, metal dopants such as Pd and Mg not only tailor the silica-based networks but also trigger interactions with H<sub>2</sub> or CO<sub>2</sub> molecules

\* Corresponding author.

E-mail address: [hqi@njtech.edu.cn](mailto:hqi@njtech.edu.cn) (H. Qi).

<https://doi.org/10.1016/j.micromeso.2020.110279>

Received 14 January 2020; Received in revised form 24 March 2020; Accepted 20 April 2020

Available online 27 April 2020

1387-1811/© 2020 Elsevier Inc. All rights reserved.

which confers the membranes with benefits for improved H<sub>2</sub>/CO<sub>2</sub> permselectivity [17–19]. Karakilic et al. [18] found Mg-doped silica membranes could show extremely high H<sub>2</sub>/CO<sub>2</sub> permselectivity (above 350). Because the doped Mg could provide abundant basic sites on the membrane pores, CO<sub>2</sub> molecules could strongly adsorb onto the sites and consequently blocked them for further permeation, resulting in a low CO<sub>2</sub> permeance of the membrane. In addition to hindering CO<sub>2</sub> permeation, doping Pd into silica-based networks could efficiently improve the H<sub>2</sub> permeance since Pd has strong adsorbability and solvability towards H<sub>2</sub> [20]. However, it should be noted that Pd doping generally shows poor compatibility with silica-based networks causing non-selective interfacial voids, which counteracts the increase of H<sub>2</sub>/CO<sub>2</sub> permselectivities [21]. Therefore, the strategy of monometallic doping is still limited to simultaneously improve H<sub>2</sub> permeance and H<sub>2</sub>/CO<sub>2</sub> permselectivity for silica-based membranes.

Apart from monometallic doping, Prof. Da Costa's group first proposed the concept of bimetallic doping and they developed a series of bimetallic doped silica membranes derived from TEOS such as the palladium-cobalt doped (Pd-Co-TEOS) [22], the iron-cobalt doped (Fe-Co-TEOS) [23,24] and the lanthanum-cobalt doped (La-Co-TEOS) [25]. Co was selected as one of components in these bimetallic doped silica membranes for the improvement of hydrothermal stability, and the introduction of Pd, Fe or La into Co-TEOS membranes further confers the membranes with improved gas separation performance. Hence, bimetallic doping (i.e. introducing two different metal dopants with specific functions) is feasible to improve the overall performance of silica-based membranes. Very recently, Zhang et al. [26] reported La-Y bimetallic doped BTESE membranes for the application of pervaporation desalination. They found that La and Y could both form Si-O-M (M represents La and Y) bonds in the BTESE-derived organosilica networks and their membranes could exhibit excellent desalination performance.

In contrast of improving the hydrothermal stability of TEOS-derived silica membranes, synergistic effects of bimetallic doping may be utilized for improving H<sub>2</sub> permeance and H<sub>2</sub>/CO<sub>2</sub> permselectivity of more hydrothermal stable BTESE-derived organosilica membranes [27,28]. Previously, we found niobium-doped BTESE (Nb-BTESE) membranes could show relatively high H<sub>2</sub>/CO<sub>2</sub> permselectivities and low H<sub>2</sub> permeances due to the dense structure caused by Nb-O-Si covalent bonds [29]. However, palladium-doped BTESE (Pd-BTESE) membranes exhibited an opposite result (i.e. poor H<sub>2</sub>/CO<sub>2</sub> permselectivity yet high H<sub>2</sub> permeance), which is attributed to the larger pore size and an enhanced H<sub>2</sub> adsorbability by Pd nanoparticles [19]. Here, we propose a novel strategy of preparing the palladium-niobium bimetallic doped organosilica (Pd-Nb-BTESE) membranes to improve both H<sub>2</sub> permeance and H<sub>2</sub>/CO<sub>2</sub> permselectivity by taking advantages of the two metal dopants. To our best knowledge, this is the first attempt that investigates the effects of bimetallic doping on gas separation performance of organosilica membranes. We hypothesized that the introduction of Pd into BTESE network increases the H<sub>2</sub> permeance due to its strong adsorption and permeability for H<sub>2</sub> and the Nb doping could maintain the permselectivity of Pd-Nb-BTESE membranes. By controlling the same doping content of Nb, we compared the structural changes and the gas separation performances of the Pd-Nb-BTESE membranes prepared with different Pd doping content. This work may provide useful insights into designing high-performance silica-based membranes for H<sub>2</sub>/CO<sub>2</sub> separation.

## 2. Experimental

### 2.1. Synthesis of Pd-Nb-BTESE sols

1,2-bis (triethoxysilyl) ethane (BTESE, purity 97%, ABCR) was used as precursor. Niobium penta (n) butoxide (NPB, purity 99%, ABCR) and palladium chloride (PdCl<sub>2</sub>, purity 98%, Meryer) were used as Nb and Pd sources, respectively. To synthesize Pd-Nb-BTESE sols, 5 mL BTESE and 5 mL ethanol anhydrous (EtOH, purity 99.9%, Merck) were first mixed

in a nitrogen glove-box. 0.5 mL hydrochloric acid solution (1 mol L<sup>-1</sup>) was drop-wise added into the BTESE-ethanol mixture under vigorous stirring in an ice bath. The mixture was then refluxed in a water bath at 60 °C for 90 min to obtain BTESE sol. Subsequently, a mixture of 3.75 mL NPB, 25 mL ethanol and 0.3 mL HCl solution (1 mol L<sup>-1</sup>) was drop-wise added into the BTESE sol. The Nb-containing mixture was then refluxed at 60 °C for an additional 90 min to obtain Nb-BTESE sol. Next, 0.2368 g PdCl<sub>2</sub> was dissolved with 0.25 mL concentrated hydrochloric acid (HCl, 36.46 wt%) in a water bath at 60 °C for 40 min. Finally, the PdCl<sub>2</sub> solution by diluting with 25 mL ethanol and as-prepared Nb-BTESE sol were mixed and then refluxed in a water bath at 60 °C for 90 min to obtain Pd-Nb-BTESE sol. The molar ratio of the as-prepared sol is n (Pd):n (Nb):n (HCl):n (H<sub>2</sub>O):n (EtOH): n (Si) = 0.05:0.33:0.14:1.63:34.81:1, which is marked as Pd-Nb-BTESE-0.05. By increasing the content of Pd, the other three sols with molar ratios of n (Pd):n (Nb):n (Si) = 0.1:0.33:1, 0.2:0.33:1 and 0.4:0.33:1 were prepared and marked as Pd-Nb-BTESE-0.1, Pd-Nb-BTESE-0.2 and Pd-Nb-BTESE-0.4, accordingly. The molar ratio of ingredients for the Pd-Nb-BTESE sols can be found in Table S1.

### 2.2. Preparation of Pd-Nb-BTESE powders and membranes

Pd-Nb-BTESE sols were dried at room temperature (25 °C) for 24 h to prepare xerogels. Then, the obtained xerogels were ground into fine powders and calcined in H<sub>2</sub>/N<sub>2</sub> (2:3, molar ratio) atmosphere at 400 °C for 3 h with the same heating and cooling rate of 0.5 °C·min<sup>-1</sup>. The powder samples were prepared and used for characterization to indicate the properties of the corresponding membranes.

Pd-Nb-BTESE membranes were prepared by single dip-coating the as-prepared sols onto home-made disk-type mesoporous  $\gamma$ -Al<sub>2</sub>O<sub>3</sub> supports (thickness: 2.5 mm, diameter: 42 mm, pore size: 5 nm). Before coating the membranes, the as-prepared sols were aged for 24 h at -20 °C. The dip-coating process was implemented at a withdrawal speed of 12 mm s<sup>-1</sup> by using a MEMDIP5 coating unit (Pervatech B.V., The Netherlands). The membranes were finally calcinated by the same procedure as the powders. The whole membrane preparation procedure is schematically given in Fig. 1.

### 2.3. Membrane characterization and gas permeation measurement

An X-ray diffractometer (XRD, MiniFlex 600, Rigaku) was used to detect phase composition of Pd-Nb-BTESE powders, using a Cu K $\alpha$  radiation operated at 40 kV and 15 mA.

Fourier transform infrared (FTIR) spectroscopy (NICOLET 8700, Thermo Nicolet Corporation) was used to analyze the chemical structures of the powders. The cross-sectional morphologies of the membranes were observed by a scanning electron microscopy (SEM, S-4800, Hitachi) with the accelerating voltage of 7 kV. Morphological characteristics of Pd-Nb-BTESE powders were carried out by a high-resolution transmission electron microscope (HRTEM, JEM-200CX, JEOL). Chemical compositions of Pd-Nb-BTESE powders were analyzed by an X-ray photoelectron spectrometer (XPS, ESCALAB250xi, Thermo Scientific) equipped with a monochromatic Al K $\alpha$  X-ray source (1486.6 eV). The microstructures of the as-prepared membranes were evaluated by characterizing their corresponding powders through N<sub>2</sub> adsorption-desorption isotherms (ASAP 2020, Micromeritics) at -196 °C. Pore size distributions were calculated by the non-local density functional theory method (NLDFT). Gas adsorption capabilities of the powders were analyzed by H<sub>2</sub> and CO<sub>2</sub> gas adsorption isotherms measured at 25 °C. Before gas adsorption measurement, samples were degassed under vacuum at 200 °C for 12 h.

Single gas permeation measurement was conducted in a dead-end modal set-up at 300 °C. Prior to measurements, temperature and pressure were kept at 300 °C and 0.3 MPa for 30 min until gas permeation reached a steady state. The single gas permeances of He, H<sub>2</sub>, CO<sub>2</sub>, N<sub>2</sub>, CH<sub>4</sub> and SF<sub>6</sub> were respectively measured. The gas permselectivity is

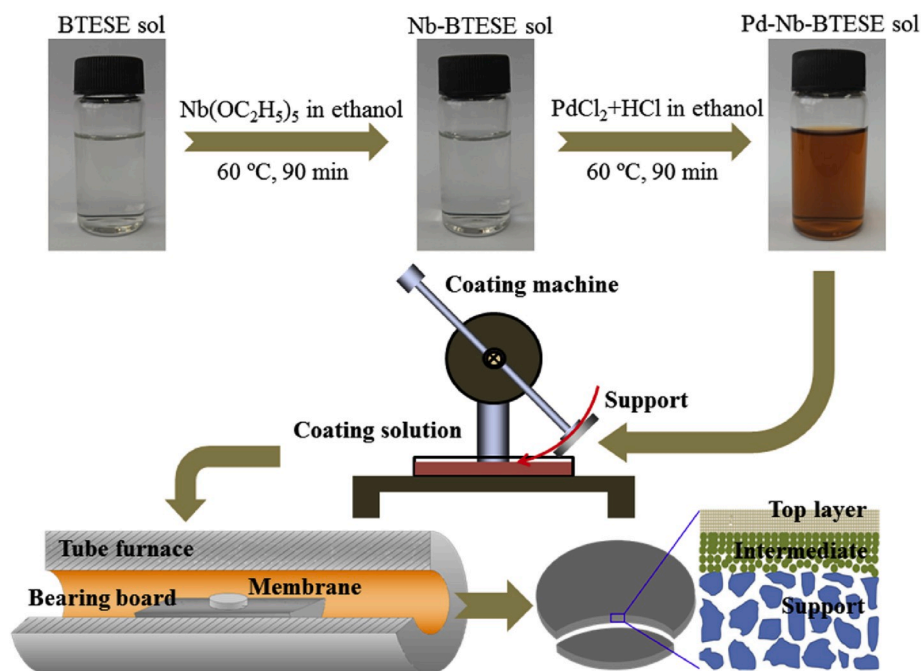


Fig. 1. Schematic illustration of the preparation process of Pd-Nb-BTESE membranes.

equal to the permeance ratio between two gases.

### 3. Results and discussion

#### 3.1. Chemical composition analysis of Pd-Nb-BTESE membranes

Fig. 2 shows the XRD patterns of Pd-Nb-BTESE powders with different Pd/Si molar ratios. No silicon- or niobium-related diffraction peaks were found for all samples, indicating that the BTESE-derived organosilica networks were amorphous. This result also implied that the doped niobium existed in the organosilica networks as an amorphous phase or the size of crystalline niobium compounds were too small to be detected by XRD, which agrees with a previous report by Pereira et al. [30]. In contrast to the doped Nb, the characteristic peaks centered at  $40.14^\circ$ ,  $46.7^\circ$  and  $68.18^\circ$   $2\theta$  correspond to (111), (200) and (220) planes suggesting the formation of Pd (0) in the four organosilica networks [31]. According to Scherer's equation, the crystal size of the doped Pd for the four membranes were similar of about 20 nm. In

addition, the relative intensity of those full Pd characteristic peaks for Pd-Nb-BTESE samples increased with the increase of Pd content, which indicates that Pd were successfully doped into the corresponding organosilica networks.

FTIR spectra were used to study the chemical states of the four Pd-Nb-BTESE membranes (Fig. 3). The four powder samples showed similar FTIR spectra, which confirm that chemical structures of the four Pd-Nb-BTESE membranes are similar. The peaks at  $3450$ ,  $1628$ ,  $1045$ ,  $775$  and  $680$   $\text{cm}^{-1}$  are assigned to Si-OH stretching vibrations, H-O-H deformation vibrations, Si-O-Si asymmetric stretching vibrations,  $-\text{CH}_2$  rocking vibrations and Si-C stretching vibrations, respectively [32,33]. The weak peak appearing at  $1410$   $\text{cm}^{-1}$  corresponds to bending asymmetric vibrations of  $-\text{CH}_2$  for Si- $\text{CH}_2$ - $\text{CH}_2$ -Si, confirming the existence of ethane-bridged silsesquioxane [32]. To study the influence of bimetal doping on chemical composition for organosilica networks, FTIR spectra of BTESE, Pd-BTESE, Nb-BTESE and Pd-Nb-BTESE were compared in

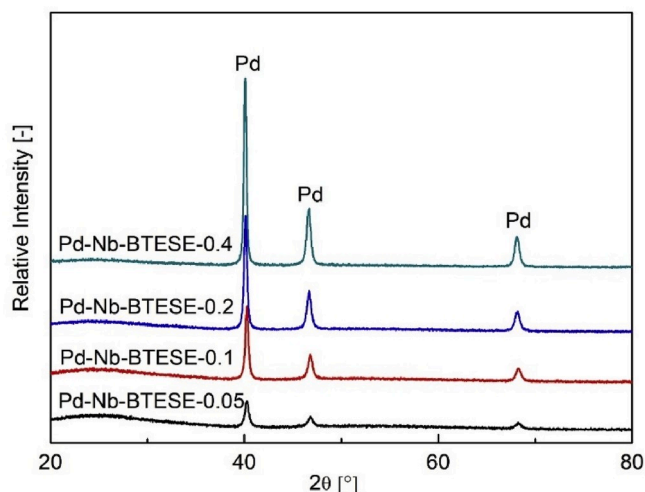


Fig. 2. XRD patterns of Pd-Nb-BTESE powders.

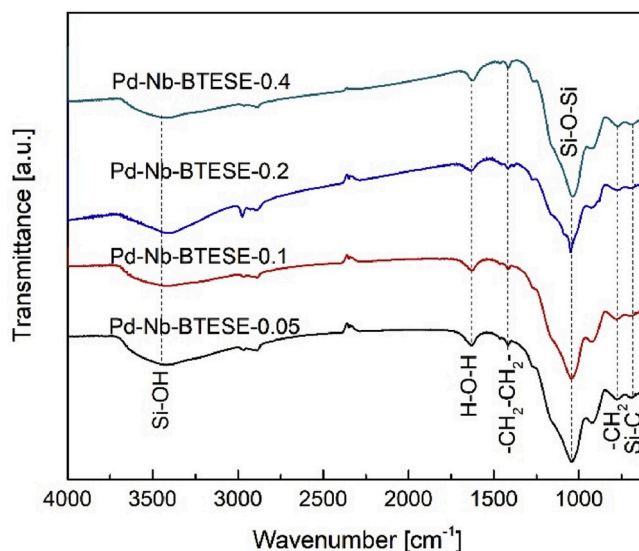


Fig. 3. FTIR spectra of Pd-Nb-BTESE powders.

**Fig. S1.** The Pd-BTESE powders exhibited the same FTIR spectra as that for the BTESE powders. However, the Nb-doped BTESE networks (i.e. the Nb-BTESE and the Pd–Nb-BTESE) showed a blue shift on the peak of Si–O–Si in FTIR spectra. The Si–O–Si vibration is very sensitive to the structural change of silica network, it could be used to indicate whether a dopant was doped into the silica network. Thus, the blue-shifted Si–O–Si peaks suggested that Nb was incorporated into organosilica networks [26].

XPS analysis of the as-prepared Pd–Nb-BTESE powders was performed to understand the chemical compositions of the Pd–Nb doped organosilica networks. Fig. 4 shows the Pd 3d and Nb 3d XPS spectra of Pd–Nb-BTESE networks with varying Pd content. Two peaks appeared at binding energies of 335.3 eV and 340.6 eV in Pd 3d spectra correspond to Pd 3d<sub>5/2</sub> and Pd 3d<sub>3/2</sub>, respectively (Fig. 4a). Both Pd 3d<sub>5/2</sub> and Pd 3d<sub>3/2</sub> peaks can be ascribed to Pd (0) [34,35], which agrees with the aforementioned XRD analysis. The core-level Nb 3d spectra of all Pd–Nb-BTESE powders showed two peaks at binding energies of 208.2 eV and 210.9 eV, which correspond to Nb 3d<sub>5/2</sub> and Nb 3d<sub>3/2</sub>, respectively (Fig. 4b). Compare with Nb 3d<sub>5/2</sub> (207.2 eV) and Nb 3d<sub>3/2</sub> (209.9 eV) peaks of pure Nb<sub>2</sub>O<sub>5</sub> powders, the two peaks of Pd–Nb-BTESE powders shifted left with higher binding energy. This result may be due to the isomorphous substitution of organosilica with Nb metal formed Nb–O–Si bonds, and the resulting lower electronic cloud density for Nb atoms [36,37]. This phenomenon was also found in other metal doped silica networks when the dopants are transition metals such as Al, Ti and Mg etc. [38]. The formation of Nb–O–Si was also confirmed by ultraviolet–visible (UV–vis) and solid-state <sup>29</sup>Si magic angle spinning nuclear magnetic resonance (<sup>29</sup>Si MAS NMR) techniques (Fig. S2 and Fig. S3).

To further study the effects of Nb doping on chemical changes in the BTESE networks, the O 1s spectra of pure BTESE, Nb<sub>2</sub>O<sub>5</sub>, and Pd–Nb-BTESE samples were compared (Fig. S4). BTESE and Nb<sub>2</sub>O<sub>5</sub> sample exhibited the O 1s peaks at 532.7 eV and 530.2 eV, corresponding to Si–O–Si and Nb–O–Nb bonds, respectively [39,40]. However, the O 1s spectra of Pd–Nb-BTESE powders can be decoupled two peaks at 532.7 eV and 531.0 eV. The detected peaks between Si–O–Si and Nb–O–Nb can be ascribed to Nb–O–Si bonds. The O 1s spectra of the four Pd–Nb-BTESE powders and the deconvolutions details of O 1s are given in Fig. 5 and Table 1. It can be seen that the percentages of Nb–O–Si for all the four samples remain constant (~7%). This result indicates that the contents of Nb–O–Si in the four Pd–Nb-BTESE networks are almost the same.

### 3.2. Morphological and structural analysis of Pd–Nb-BTESE membranes

Fig. 6 shows the TEM images of the four Pd–Nb-BTESE powders.

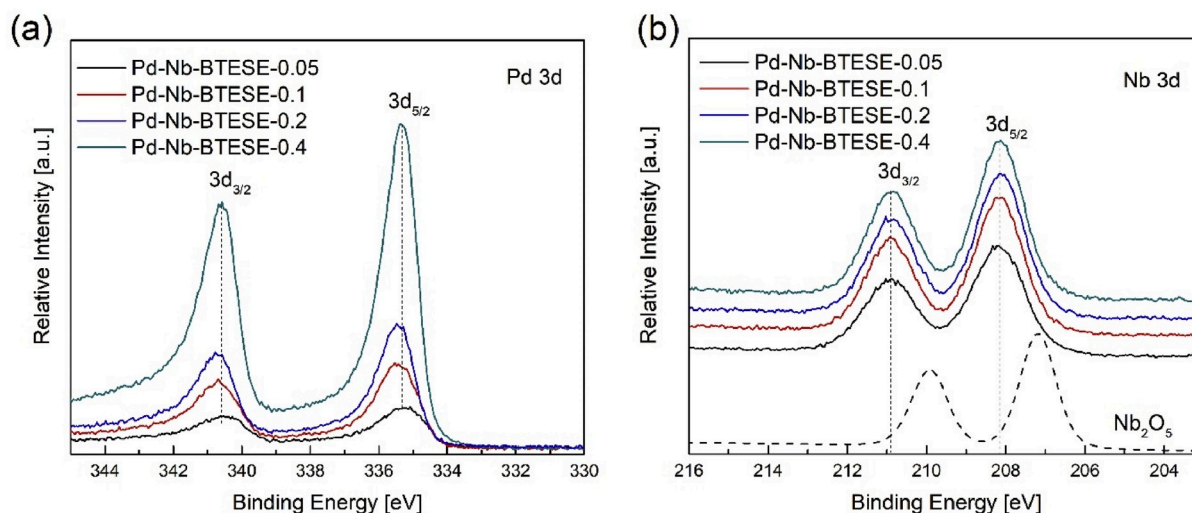


**Fig. 4.** XPS spectra for (a) Pd 3d and (b) Nb 3d of Pd–Nb-BTESE powders.

Uniformly distributed black particles with size of about 5–10 nm were clearly observed in the four organosilica networks. In Fig. 6d, the distance of lattice fringe for the black nanoparticles was 0.196 nm corresponding to (200) plane of Pd (0) [41], which confirmed that the embedded black nanoparticles in the organosilica networks were Pd nanoparticles. It was observed that the Pd nanoparticle size did not vary with the increase of the concentration of doped Pd, but a higher Pd doping content resulted in the increased density of Pd nanoparticles in the corresponding organosilica networks.

Fig. 7 shows the cross-sectional SEM images of the four Pd–Nb-BTESE membranes. All these membranes exhibit an asymmetric structure including a  $\alpha$ -Al<sub>2</sub>O<sub>3</sub> support layer, a  $\gamma$ -Al<sub>2</sub>O<sub>3</sub> intermediate layer and a Pd–Nb-BTESE separation layer. The Pd–Nb-BTESE layers of the four membranes have a similar thickness of about 170 nm. Fig. S5 shows the surface morphology of Pd–Nb-BTESE-0.4 membrane that the membrane surface is smooth and defect free.

N<sub>2</sub> adsorption-desorption experiments were conducted to determine the effects of the bimetallic doping on microstructural changes of the organosilica networks. The N<sub>2</sub> adsorption-desorption isotherms of Pd–Nb-BTESE powders are shown in Fig. 8. All samples reached high adsorption capacities rapidly at a very low relative pressure region matching well with the characteristics of type I isotherms, confirming that the Pd–Nb-BTESE membranes have microporous structures [42]. However, Pd–Nb-BTESE-0.1, 0.2 and 0.4 showed small hysteric loops at the 0.4–0.7 relative pressure indicating some mesopores exist in the Pd–Nb-BTESE networks. The detailed pore structure information of Pd–Nb-BTESE powders is given in Table 2. Pd–Nb-BTESE-0.05 powders exhibited the highest Brunauer-Emmett-Teller surface area ( $S_{\text{BET}}$ , 233 m<sup>2</sup> g<sup>-1</sup>) and the largest total pore volume ( $V_{\text{total}}$ , 0.129 cm<sup>3</sup> g<sup>-1</sup>). As Pd doping content increased,  $S_{\text{BET}}$  and  $V_{\text{total}}$  of the prepared Pd–Nb-BTESE powders both showed a decreasing trend. When the n (Pd): n (Si) rose to 0.4, the  $S_{\text{BET}}$  and  $V_{\text{total}}$  values of the sample were 177 m<sup>2</sup> g<sup>-1</sup> and 0.108 cm<sup>3</sup> g<sup>-1</sup>, respectively. This result could be attributed to the increased density of Pd nanoparticles in Pd–Nb-BTESE networks. Pd nanoparticles could competitively occupy pore volume in the Pd–Nb-BTESE networks, resulting in the decrease of  $S_{\text{BET}}$  and  $V_{\text{total}}$ .

In addition, the N<sub>2</sub> adsorption-desorption isotherms of BTESE, Pd-BTESE and Nb-BTESE powders were shown in Fig. S6. The N<sub>2</sub> adsorption-desorption isotherm of BTESE powders shows a type I isotherms suggesting the microporous structure. Compared with the BTESE powders, the Pd-BTESE powder exhibits a higher N<sub>2</sub> adsorption capacity and has a large hysteric loop at the range of 0.4–0.9 relative pressure, indicating some mesopores exist in the Pd-BTESE network. This result implied that doping Pd led to a larger pore size of the BTESE network. The

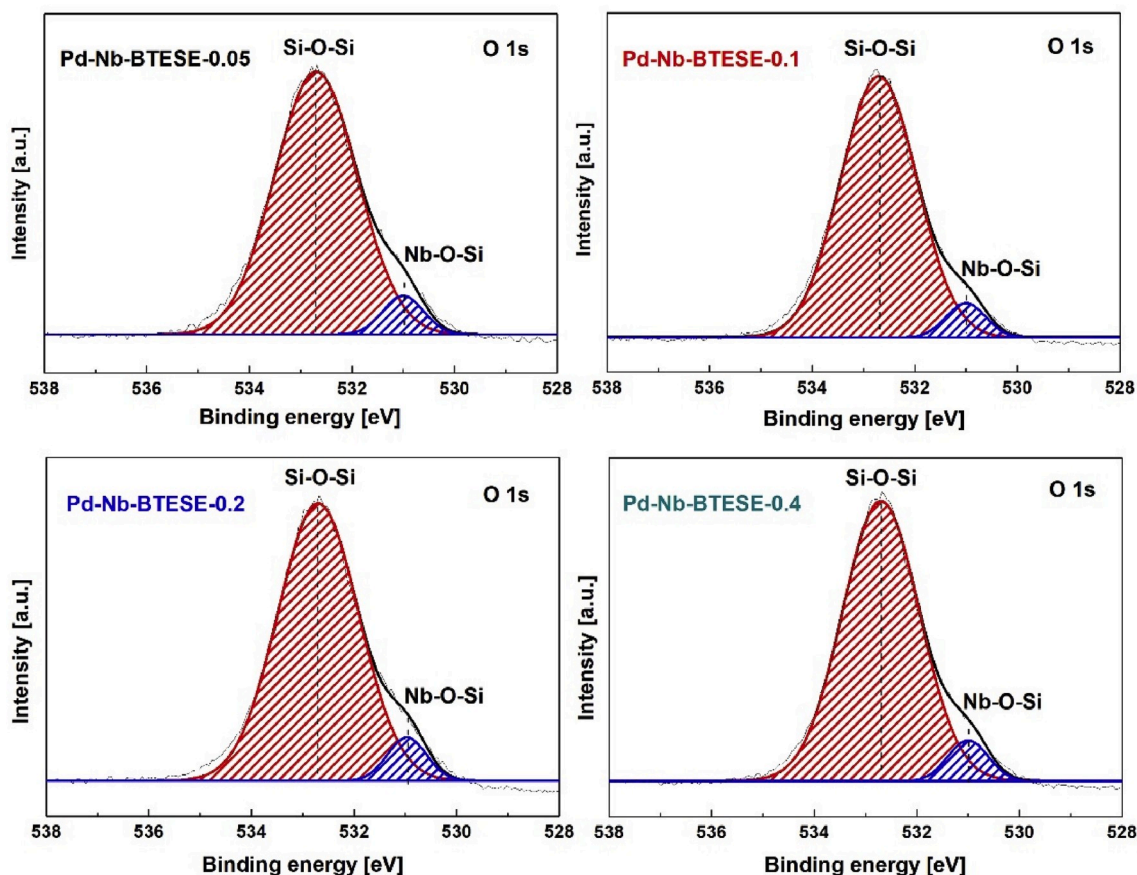


Fig. 5. Deconvolution of the XPS O1s peak of Pd–Nb-BTESE powders.

**Table 1**  
XPS deconvolution details of O1s peaks of Pd–Nb-BTESE powders.

Sample	BE (eV)	FWHM (eV)	Assignment	Percentage (%)
Pd–Nb-BTESE-0.05	532.7	1.9	Si–O–Si	92.9
	531	0.94	Nb–O–Si	7.1
Pd–Nb-BTESE-0.1	532.7	1.75	Si–O–Si	93.0
	531	0.91	Nb–O–Si	7.0
Pd–Nb-BTESE-0.2	532.7	1.85	Si–O–Si	92.9
	531	0.9	Nb–O–Si	7.1
Pd–Nb-BTESE-0.4	532.7	1.76	Si–O–Si	92.8
	531	0.94	Nb–O–Si	7.2

Note: BE and FWHM represent binding energy and full width at half maxima, respectively.

N<sub>2</sub> adsorption-desorption isotherm of Nb-BTESE powders is almost undetectable. The detailed  $S_{\text{BET}}$  and  $V_{\text{total}}$  of the three samples are given in Table S2. The  $S_{\text{BET}}$  and  $V_{\text{total}}$  of Nb-doped BTESE powders are not available due to its dense structure. In contrast to the Nb-BTESE networks, the Pd-BTESE powders showed larger  $S_{\text{BET}}$  of 507 m<sup>2</sup> g<sup>−1</sup> and  $V_{\text{total}}$  of 0.354 cm<sup>3</sup> g<sup>−1</sup> than those of pure BTESE ( $S_{\text{BET}}$  of 360 m<sup>2</sup> g<sup>−1</sup> and  $V_{\text{total}}$  of 0.205 cm<sup>3</sup> g<sup>−1</sup>). These results are in agreement with our previous monometallic doped BTESE work [19,29]. Therefore, compared with the two types of monometallic doped BTESE networks, the relatively moderate  $S_{\text{BET}}$  and  $V_{\text{total}}$  of the as-prepared Pd–Nb-BTESE networks suggested that Pd–Nb bimetallic doping may present a better balance between the permeance and permselectivity in H<sub>2</sub>/CO<sub>2</sub> separation.

To further explore the porous structures of the as-prepared membranes, the pore size distributions (PSDs) of Pd–Nb-BTESE powders were calculated by the NLDFT method (Fig. 9). The pore size distributions of all samples are multimodal containing a main microporous region and a

partial mesoporous region, indicating that micropores are predominant and a small amount of mesopores exist in these networks. The main pore sizes of the Pd–Nb-BTESE networks were centered at 6.01, 5.94, 5.84 and 5.96 Å as the n (Pd): n (Si) increased from 0.05 to 0.4, respectively. When n (Pd): n(Si) ratio is below 0.2, the pore sizes of the corresponding networks decrease as the Pd doping contents increase. However, at a high Pd doping content (n (Pd): n(Si) = 0.4), the pore size of Pd–Nb-BTESE-0.4 sample increases, which may be ascribed to the formation of larger pores caused by the high density of Pd nanoparticles.

### 3.3. Gas separation performance of Pd–Nb-BTESE membranes

Fig. 10 shows the kinetic diameter of gases dependency on single gas permeances for Pd–Nb-BTESE membranes. The permeances of the four Pd–Nb-BTESE membranes exhibited a decreasing tendency as the kinetic diameter of gases increases, except for H<sub>2</sub> permeance of Pd–Nb-BTESE-0.4 membrane. This result indicated that Pd–Nb-BTESE membranes possess molecular sieving characteristics. Among the four membranes, Pd–Nb-BTESE-0.05 membrane showed the highest gas permeances to all tested gases except for H<sub>2</sub>. Both Pd–Nb-BTESE-0.1 and Pd–Nb-BTESE-0.2 membranes showed relatively low permeances to the tested gases. Pd–Nb-BTESE-0.2 membrane exhibited the lowest permeances to all gases, which agrees with the aforementioned pore size analysis. Interestingly, He, CO<sub>2</sub>, N<sub>2</sub> and CH<sub>4</sub> permeances of Pd–Nb-BTESE-0.4 membrane were between those of Pd–Nb-BTESE-0.2 and Pd–Nb-BTESE-0.05, and Pd–Nb-BTESE-0.4 membrane showed the highest H<sub>2</sub> permeance.

Table S3 lists the permeances of H<sub>2</sub> and CO<sub>2</sub> and the H<sub>2</sub>/CO<sub>2</sub> permselectivities for the as-prepared Pd–Nb-BTESE membranes. All H<sub>2</sub>/CO<sub>2</sub> permselectivities of the four membranes are much greater than the Knudsen diffusion factor (4.7), suggesting that all the prepared Pd–Nb-

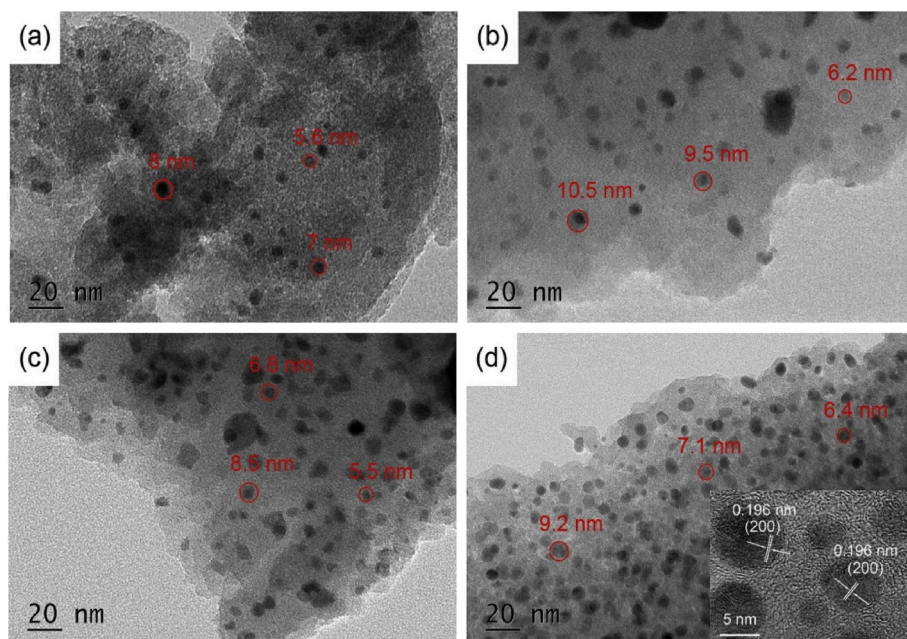


Fig. 6. HRTEM images of (a) Pd-Nb-BTESE-0.05, (b) Pd-Nb-BTESE-0.1, (c) Pd-Nb-BTESE-0.2 and (d) Pd-Nb-BTESE-0.4 powders (the inset of Fig. 6d is the HRTEM image for Pd nanoparticles in high-magnification).

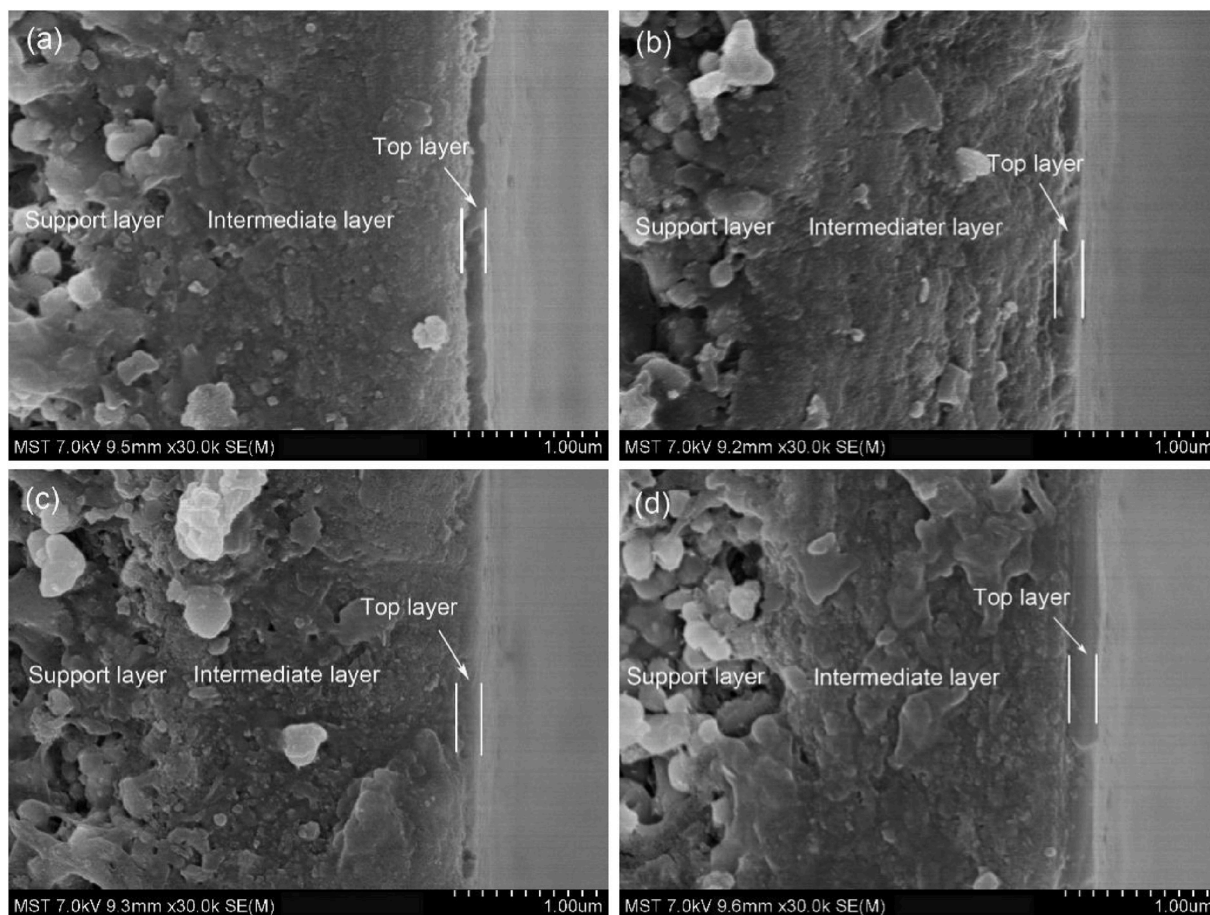


Fig. 7. SEM images of (a) Pd-Nb-BTESE-0.05, (b) Pd-Nb-BTESE-0.1, (c) Pd-Nb-BTESE-0.2, (d) Pd-Nb-BTESE-0.4 membranes.

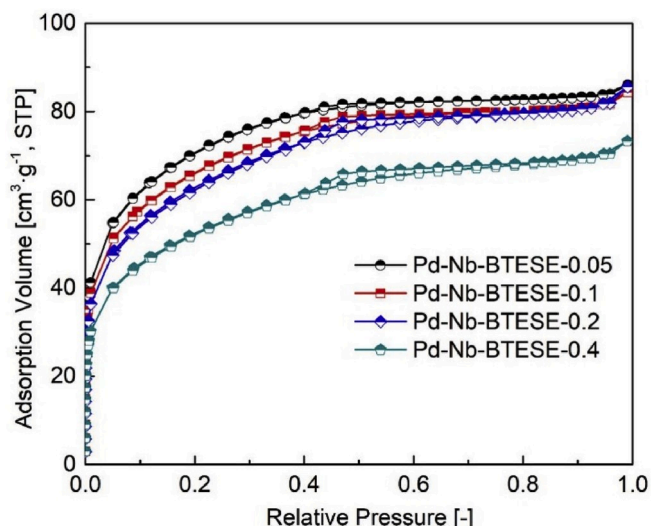


Fig. 8. N<sub>2</sub> adsorption-desorption isotherms of Pd-Nb-BTESE powders.

Table 2

Pore structure data of Pd-Nb-BTESE powders.

Sample	S <sub>BET</sub> (m <sup>2</sup> ·g <sup>-1</sup> )	V <sub>total</sub> (cm <sup>3</sup> ·g <sup>-1</sup> )
Pd-Nb-BTESE-0.05	233	0.129
Pd-Nb-BTESE-0.1	223	0.126
Pd-Nb-BTESE-0.2	214	0.124
Pd-Nb-BTESE-0.4	177	0.108

Note: S<sub>BET</sub> and V<sub>total</sub> represent Brunauer-Emmett-Teller (BET) surface area and total pore volume, respectively.

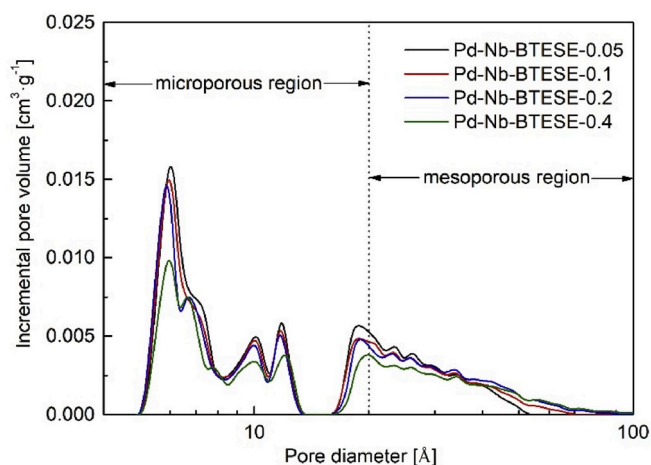


Fig. 9. Pore size distributions of Pd-Nb-BTESE powders calculated by NLDFT method.

BTESE membranes could be used for H<sub>2</sub>/CO<sub>2</sub> separation. Pd-Nb-BTESE-0.05 membranes showed H<sub>2</sub> permeance of  $8.7 \times 10^{-8} \text{ mol m}^{-2} \text{ s}^{-1} \cdot \text{Pa}^{-1}$  and H<sub>2</sub>/CO<sub>2</sub> permselectivity of 40, respectively. Although H<sub>2</sub> permeances of Pd-Nb-BTESE-0.1 and Pd-Nb-BTESE-0.2 membranes did not increase, H<sub>2</sub>/CO<sub>2</sub> permselectivities of the two membranes reached up to 53 and 54, respectively. Pd-Nb-BTESE-0.4 membrane not only showed the highest H<sub>2</sub> permeance ( $1.12 \times 10^{-7} \text{ mol m}^{-2} \text{ s}^{-1} \cdot \text{Pa}^{-1}$ ), but also the highest H<sub>2</sub>/CO<sub>2</sub> permselectivity (107). The H<sub>2</sub> and CO<sub>2</sub> permeation mechanisms of Pd-Nb-BTESE-0.4 membrane have been discussed in Supporting Information (See Fig. S7). The H<sub>2</sub> molecules pass through Pd-Nb-BTESE-0.4 membrane by activated diffusion, while CO<sub>2</sub> molecules through the membrane are dominated by surface diffusion

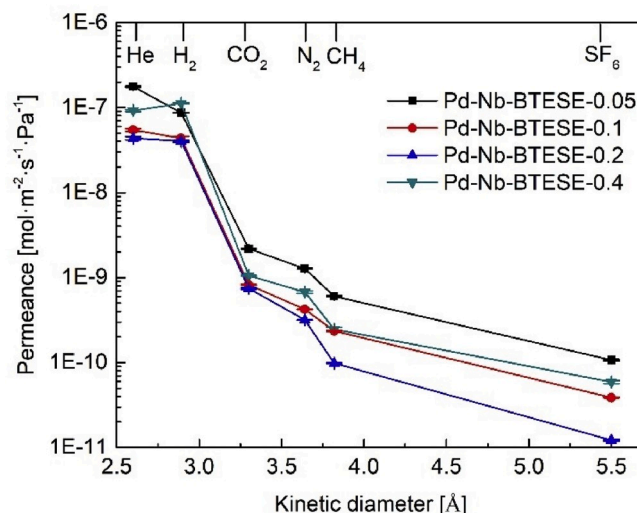


Fig. 10. Gas permeances of Pd-Nb-BTESE membranes measured at 300 °C.

mechanism. The Pd-Nb-BTESE-0.4 membrane showed stable performance and good reproducibility (Fig. S8 and Fig. S9).

To further explain the results of single gas permeation of the as-prepared Pd-Nb-BTESE membranes, H<sub>2</sub> and CO<sub>2</sub> adsorption experiments for the corresponding Pd-Nb-BTESE powders were conducted. The four Pd-Nb-BTESE samples with different Pd-doping contents exhibited different H<sub>2</sub> adsorption isotherms, while CO<sub>2</sub> adsorption isotherms for all samples almost remained the same (Fig. 11). Obviously, the H<sub>2</sub> adsorption isotherms of all Pd-Nb-BTESE powders experienced dramatically increase at low absolute pressures (~50 mm Hg), and H<sub>2</sub> adsorbabilities gradually became stronger with the increase of Pd doping content. This result suggested that the high density Pd nanoparticles in Pd-Nb-BTESE-0.4 network dominated its H<sub>2</sub> adsorption process, which indirectly explains that Pd-Nb-BTESE-0.4 membrane has the highest H<sub>2</sub> permeance. In addition, to further reveal the H<sub>2</sub> adsorbability of Pd in the organosilica network, the H<sub>2</sub> adsorption isotherms of Pd-BTESE, Nb-BTESE and BTESE were provided in Fig. S10. Both Nb-BTESE and BTESE samples showed a very low H<sub>2</sub> adsorption capacity, suggesting that Nb and BTESE cannot contribute to the high H<sub>2</sub> adsorption capacity of Pd-Nb-BTESE powders. However, Pd-BTESE sample showed a high H<sub>2</sub> adsorption capacity and the characteristic of H<sub>2</sub> adsorption isotherms is same as the Pd-Nb-BTESE powders. This

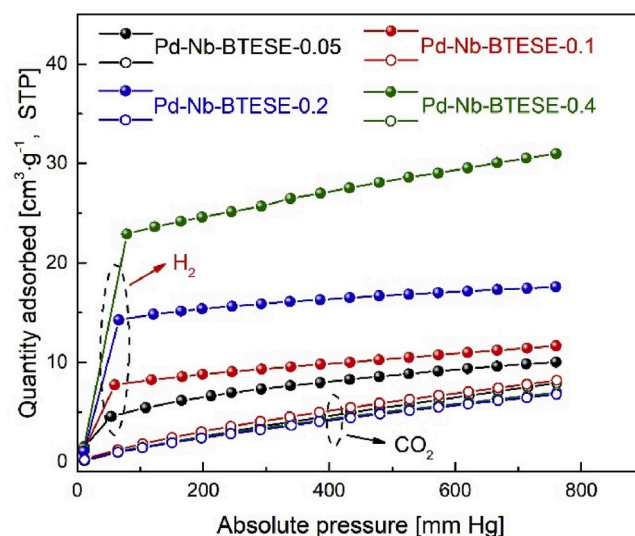


Fig. 11. H<sub>2</sub> and CO<sub>2</sub> adsorption isotherms of Pd-Nb-BTESE powders.

result demonstrated that the doped Pd govern the  $H_2$  adsorption capacities of the Pd–Nb–BTESE samples, which agrees with previous reports that metal Pd generally exhibits strong adsorbability toward  $H_2$  for Pd-doped organosilica membranes [19].

According to the deep understanding of monometallic doped BTESE membranes (i.e. Pd- or Nb-doped membranes) and new findings presented in this work, the structural evolution of Pd–Nb–BTESE network from pure BTESE is schematically illustrated in Fig. 12. The pure BTESE-derived organosilica networks with relatively high pore volume and large pore size usually exhibit high  $H_2$  permeances and low  $H_2/CO_2$  permselectivities [43]. The introduction of Nb could form new covalent bonds Nb–O–Si into the BTESE-derived networks and make the structures become much denser [29]. As a result,  $H_2$  permeances of Nb-doped BTESE membranes are often very low, while of these membranes always exhibit high  $H_2/CO_2$  permselectivities. The mechanism of bimetallic doing into BTESE network is that when incorporated Pd into Nb-induced dense organosilica networks, the formed Pd nanoparticles can not only inhibit excessive densification of the Nb-doped networks but also functionalize the networks with  $H_2$  preference. The increased Pd content conferred Pd–Nb–BTESE membranes a stronger  $H_2$  adsorbability which is beneficial to improve the  $H_2$  permeance. Therefore, we believe that the synergetic effects of bimetallic doping with Pd and Nb confers BTESE-derived organosilica membranes with moderate structures and excellent  $H_2$  separation performance.

Fig. 13 compares the  $H_2/CO_2$  separation performance ( $H_2$  permeance and  $H_2/CO_2$  permselectivity) of the as-prepared Pd–Nb–BTESE membranes with other silica-based membranes reported in literature, where the commonly adopted upper bound 2008 is marked [44]. The detailed operational parameters and the separation performance of those membranes are provided in Table S4. It can be seen that the traditional  $SiO_2$  membranes exhibit the excellent  $H_2/CO_2$  separation performance, but it is well-known that these membranes suffer from poor hydrothermal stability under steam conditions for practical applications [5]. Only Co– $SiO_2$  membrane was tested with  $H_2/CO_2$  binary gas, which shows a  $H_2/CO_2$  selectivity of 40 but an extremely low  $H_2$  permeance [45]. Compared with  $SiO_2$  membranes, organosilica-based membranes generally exhibit enhanced hydrothermal stability but their  $H_2/CO_2$  separation performance are not ideal enough. Most pure BTESE-derived membranes exhibited low  $H_2/CO_2$  permselectivities that are below Knudsen diffusion factor (4.7) [43,46]. Monometallic doping strategy was found to be effective for improving either  $H_2$  permeance or  $H_2/CO_2$  permselectivity of BTESE-derived membranes [16,19,28,29,47]. In addition, although the bimetallic doped TEOS-derived silica membranes

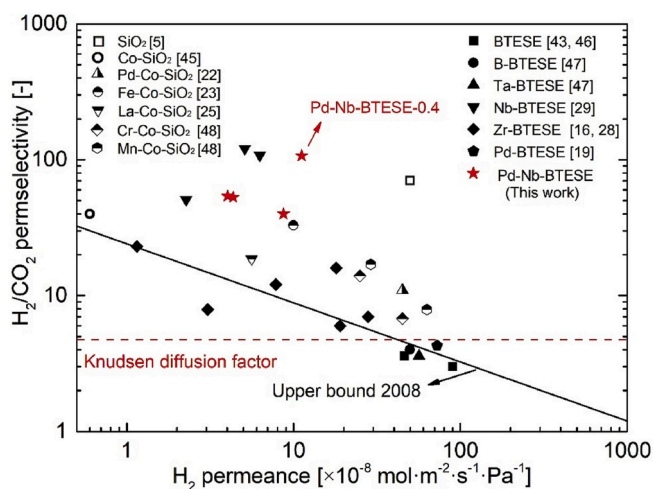


Fig. 13. Comparison of  $H_2/CO_2$  separation performance for Pd–Nb–BTESE membranes prepared in this work with that for other membranes reported in literature (the upper bound 2008 line is drawn by converting permeability to permeance assuming the membranes thickness of 100 nm).

exhibited improved hydrothermal stability, they did not display impressive  $H_2/CO_2$  separation performance that their permselectivities were close to upper bound 2008 [22,23,25,48]. We note that the  $H_2/CO_2$  permselectivities of all the Pd–Nb–BTESE membranes in this work are far above the upper bound 2008, and the optimal membrane (i.e. Pd–Nb–BTESE-0.4) showed a very competitive  $H_2/CO_2$  separation performance compared with that of reported silica-based membranes in literature.

#### 4. Conclusions

Bimetallic doped BTESE-derived organosilica membranes were prepared by using the sol-gel method and the synergetic effects of Pd–Nb bimetallic doping on the organosilica networks were investigated. By controlling the same Nb doping content, the influences of different Pd doping contents ( $n$  (Pd):  $n$  (Si) = 0.05, 0.1, 0.2 and 0.4) on microstructures and  $H_2/CO_2$  separation performances of the as-prepared Pd–Nb–BTESE membranes were compared. As evidenced by a series of characterization, the same amount of Nb was first covalently incorporated into the four networks through the formation Nb–O–Si bonds, while metal Pd was doped into the networks in the form of nanoparticles. These Pd nanoparticles with size of  $\sim 5$ – $10$  nm were uniformly embedded into the as-prepared Pd–Nb–BTESE networks, for which the densities of Pd nanoparticles increases with the Pd doping content increases.

The bimetallic doping mechanism for the Pd–Nb–BTESE was established. Compared with Pd- or Nb-doped membranes, the four bimetallic doped membranes showed more moderate microporous structures and improved  $H_2/CO_2$  separation performances. We found that tuning the Pd doping content was crucial for tailoring the pore sizes and the  $H_2$  adsorption capacities of the Pd–Nb–BTESE networks, which eventually contributes to the  $H_2/CO_2$  separation performance of the corresponding membranes.

In addition,  $H_2/CO_2$  separation performances of the four Pd–Nb–BTESE membranes are all far above the upper bound 2008. Pd–Nb–BTESE-0.4 membrane exhibits superior  $H_2/CO_2$  separation performance with  $H_2$  permeance of  $1.12 \times 10^{-7} \text{ mol m}^{-2} \text{ s}^{-1} \cdot \text{Pa}^{-1}$  and  $H_2/CO_2$  permselectivity of 107, which is very competitive over that of reported silica-based membranes in literature. Thus, this work may signify an important step toward designing and developing high-performance organosilica membranes that challenge trade-off effects for practical  $H_2/CO_2$  separation.

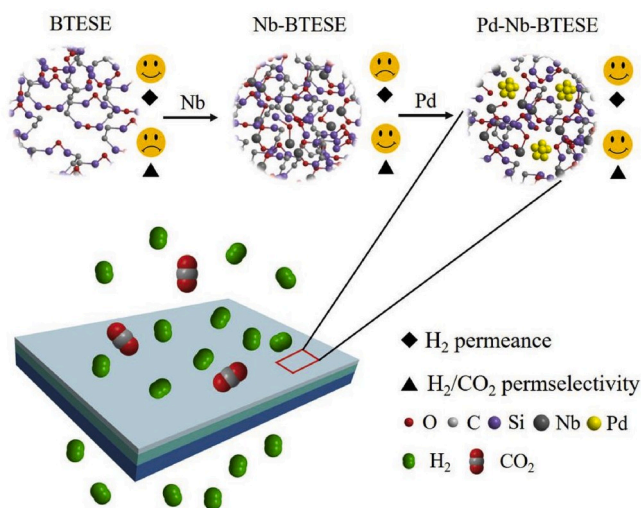


Fig. 12. Schematic illustration of the hypothetical structures for Pd–Nb–BTESE networks for  $H_2/CO_2$  separation.

## Declaration of competing interest

The authors declare that they have no known competing financial interests or personal relationships that could have appeared to influence the work reported in this paper.

## CRediT authorship contribution statement

**Hengfei Zhang:** Conceptualization, Methodology, Investigation, Formal analysis, Data curation, Writing - original draft. **Yibin Wei:** Methodology, Investigation, Formal analysis, Writing - review & editing. **Hong Qi:** Investigation, Resources, Supervision, Writing - review & editing.

## Acknowledgments

This work is supported by the National Natural Science Foundation of China (21490581), China Petroleum & Chemical Corporation (317008-6) and Guangxi Innovation Driven Development Foundation (AA17204092).

## Appendix A. Supplementary data

Supplementary data to this article can be found online at <https://doi.org/10.1016/j.micromeso.2020.110279>.

## References

- [1] S.N. Paglieri, J.D. Way, Innovations in palladium membrane research, *Separ. Purif. Methods* 31 (2002) 1–169.
- [2] Y.S. Lin, Microporous and dense inorganic membranes: current status and prospective, *Separ. Purif. Technol.* 25 (2015) 39–55.
- [3] Y. Yoshino, T. Suzuki, B.N. Nair, H. Taguchi, N. Itoh, Development of tubular substrates, silica based membranes and membrane modules for hydrogen separation at high temperature, *J. Membr. Sci.* 267 (2005) 8–17.
- [4] R.J.R. Uhlhorn, M.H.B.J. Huis In't Veld, K. Keizer, A.J. Burggraaf, High permselectivities of microporous silica-modified  $\gamma$ -alumina membranes, *J. Mater. Sci. Lett.* 8 (1989) 1135–1138.
- [5] R.M. de Vos, H. Verweij, High-selectivity, high-flux silica membranes for gas separation, *Science* 279 (1998) 1710–1711.
- [6] K.R. Iler, *The Chemistry of Silica*, Wiley & Sons Inc., New York, USA, 1979.
- [7] J. Campaniello, C.W.R. Engelen, W.G. Haije, P. Pex, J.F. Vente, Long-term pervaporation performance of microporous methylated silica membranes, *Chem. Commun.* (2004) 834–835.
- [8] H.L. Castricum, R. Kreiter, H.M.V. Veen, D.H.A. Blank, J.F. Vente, J.E.T. Elshof, High-performance hybrid pervaporation membranes with superior hydrothermal and acid stability, *J. Membr. Sci.* 324 (2008) 111–118.
- [9] I. Agirre, P.L. Arias, H.L. Castricum, M. Creatore, J.E.T. Elshof, G.G. Paradis, P.H. T. Ngamou, H.M.V. Veen, J.F. Vente, Hybrid organosilica membranes and processes: status and outlook, *Separ. Purif. Technol.* 121 (2014) 2–12.
- [10] M. Kanezashi, K. Yada, T. Yoshioka, T. Tsuru, Design of silica networks for development of highly permeable hydrogen separation membranes with hydrothermal stability, *J. Am. Chem. Soc.* 131 (2009) 414–415.
- [11] N.W. Ockwig, T.M. Nenoff, Membranes for hydrogen separation, *Chem. Rev.* 107 (2007) 4078–4110.
- [12] S.A. And, S. Fernando, Hydrogen membrane separation techniques, *Ind. Eng. Chem. Res.* 45 (2006) 875–881.
- [13] A. Brunetti, F. Scura, G. Barbieri, E. Drioli, Membrane technologies for CO<sub>2</sub> separation, *J. Membr. Sci.* 359 (2010) 115–125.
- [14] M. Kanezashi, S. Miyauchi, H. Nagasawa, T. Yoshioka, T. Tsuru, Gas permeation properties through Al-doped organosilica membranes with controlled network size, *J. Membr. Sci.* 466 (2014) 246–252.
- [15] V. Boffa, D.H.A. Blank, J.E.T. Elshof, Hydrothermal stability of microporous silica and niobia-silica membranes, *J. Membr. Sci.* 319 (2008) 256–263.
- [16] M.T. Hove, A. Nijmeijer, L. Winnubst, Facile synthesis of zirconia doped hybrid organic inorganic silica membranes, *Separ. Purif. Technol.* 147 (2015) 372–378.
- [17] M. Kanezashi, M. Sano, T. Yoshioka, T. Tsuru, Extremely thin Pd-silica mixed-matrix membranes with nano-dispersion for improved hydrogen permeability, *Chem. Commun.* 46 (2010) 6171–6173.
- [18] P. Karakiliç, C. Huiskes, M.W.J. Luiten-Olieman, A. Nijmeijer, L. Winnubst, Sol-gel processed magnesium-doped silica membranes with improved H<sub>2</sub>/CO<sub>2</sub> separation, *J. Membr. Sci.* 543 (2017) 195–201.
- [19] H. Song, S. Zhao, J. Lei, C. Wang, H. Qi, Pd-doped organosilica membrane with enhanced gas permeability and hydrothermal stability for gas separation, *J. Mater. Sci.* 51 (2016) 6275–6286.
- [20] S. Yun, S.T. Oyama, Correlations in palladium membranes for hydrogen separation: a review, *J. Membr. Sci.* 375 (2011) 28–45.
- [21] M. Kanezashi, D. Fuchigami, T. Yoshioka, T. Tsuru, Control of Pd dispersion in sol-gel-derived amorphous silica membranes for hydrogen separation at high temperatures, *J. Membr. Sci.* 439 (2013) 78–86.
- [22] B. Ballinger, J. Motuzas, S. Smart, J.C. Diniz da Costa, Palladium cobalt binary doping of molecular sieving silica membranes, *J. Membr. Sci.* 451 (2014) 185–191.
- [23] A. Darmawan, J. Motuzas, S. Smart, A. Julbe, J.C. Diniz da Costa, Binary iron cobalt oxide silica membrane for gas separation, *J. Membr. Sci.* 474 (2015) 32–38.
- [24] A. Darmawan, J. Motuzas, S. Smart, A. Julbe, J.C. Diniz da Costa, Gas permeation redox effect of binary iron oxide/cobalt oxide silica membranes, *Separ. Purif. Technol.* 171 (2016) 248–255.
- [25] B. Ballinger, J. Motuzas, S. Smart, J.C. Diniz da Costa, Gas permeation redox effect on binary lanthanum cobalt silica membranes with enhanced silicate formation, *J. Membr. Sci.* 489 (2015) 220–226.
- [26] H.-Y. Zhang, J.-L. Wen, Q. Shao, A. Yuan, H.-T. Ren, F.-Y. Luo, X.-L. Zhang, Fabrication of La/Y-codoped microporous organosilica membranes for high-performance pervaporation desalination, *J. Membr. Sci.* 584 (2019) 353–363.
- [27] H.L. Castricum, A. Sah, R. Kreiter, D.H. Blank, J.F. Vente, E. Johan, Hydrothermally stable molecular separation membranes from organically linked silica, *J. Mater. Chem.* 18 (2008) 2150–2158.
- [28] H. Song, S. Zhao, J. Chen, H. Qi, Hydrothermally stable Zr-doped organosilica membranes for H<sub>2</sub>/CO<sub>2</sub> separation, *Microporous Mesoporous Mater.* 224 (2016) 277–284.
- [29] H. Qi, H. Chen, L. Li, G. Zhu, N. Xu, Effect of Nb content on hydrothermal stability of a novel ethylene-bridged silsesquioxane molecular sieving membrane for H<sub>2</sub>/CO<sub>2</sub> separation, *J. Membr. Sci.* 421–422 (2012) 190–200.
- [30] E.B. Pereira, M.M. Pereira, Y. Lam, C.A. Perez, M. Schmal, Synthesis and characterization of niobium oxide layers on silica and the interaction with nickel, *Appl. Catal., A* 197 (2000) 99–106.
- [31] D.-T. Phan, G.-S. Chung, Characteristics of resistivity-type hydrogen sensing based on palladium-graphene nanocomposites, *Int. J. Hydrogen Energy* 39 (2014) 620–629.
- [32] P.H.T. Ngamou, J.P. Overbeek, R. Kreiter, H.M.V. Veen, J.F. Vente, I.M. Wienk, P. F. Cuperus, M. Creatore, Plasma-deposited hybrid silica membranes with a controlled retention of organic bridges, *J. Mater. Chem.* 1 (2013) 5567–5576.
- [33] R. Al-Oweini, H. El-Rassy, Synthesis and characterization by FTIR spectroscopy of silica aerogels prepared using several Si(OR)<sub>4</sub> and R''Si(OR)<sub>3</sub> precursors, *J. Mol. Struct.* 919 (2009) 140–145.
- [34] S.L. Chang, J.W. Anderegg, P.A. Thiel, Surface oxidation of an Al-Pd-Mn quasicrystal, characterized by X-ray photoelectron spectroscopy, *J. Non-Cryst. Solids* 195 (1996) 95–101.
- [35] J. Li, W. Li, G. Liu, Y. Deng, J. Yang, Y. Chen, Tricobalt tetraoxide-supported palladium catalyst derived from metal organic frameworks for complete benzene oxidation, *Catal. Lett.* 146 (2016) 1300–1308.
- [36] H. Yue, X. Yan, S.J. Ding, H.L. Lu, Q.Q. Sun, D.W. Zhang, Z. Chen, Thermal stability of atomic-layer-deposited ultra-thin niobium oxide film on Si (1 0 0), *Appl. Surf. Sci.* 257 (2011) 7305–7309.
- [37] S. Damyanova, L. Dimitrov, L. Petrov, P. Grange, Effect of niobium on the surface properties of Nb<sub>2</sub>O<sub>5</sub>-SiO<sub>2</sub>-supported Mo catalysts, *Appl. Surf. Sci.* 214 (2003) 68–74.
- [38] L. Zhang, J.Y. Ying, Synthesis and characterization of mesoporous niobium-doped silica molecular sieves, *AIChE J.* 43 (1997) 2793–2801.
- [39] E.B. Pereira, M.M. Pereira, Y.L. Lam, C.A.C. Perez, M. Schmal, Synthesis and characterization of niobium oxide layers on silica and the interaction with nickel, *Appl. Catal., A* 197 (2000) 99–106.
- [40] L. Dragone, P. Moggi, G. Predieri, R. Zanoni, Niobia and silica-niobia catalysts from sol-gel synthesis: an X-ray photoelectron spectroscopic characterization, *Appl. Surf. Sci.* 187 (2002) 82–88.
- [41] S. Penner, D. Wang, B. Jenewein, H. Gabasch, B. Klötzer, A. Knop-Gericke, R. Schlögl, K. Hayek, Growth and decomposition of aligned and ordered PdO nanoparticles, *J. Chem. Phys.* 125 (2006), 094703.
- [42] M. Thommes, K. Kaneko, A.V. Neimark, J.P. Olivier, F. Rodriguez-Reinoso, J. Rouquerol, K.S.W. Sing, Physisorption of gases, with special reference to the evaluation of surface area and pore size distribution (IUPAC Technical Report), *Pure Appl. Chem.* 87 (2015) 1051–1069.
- [43] H.F. Qureshi, A. Nijmeijer, L. Winnubst, Influence of sol-gel process parameters on the micro-structure and performance of hybrid silica membranes, *J. Membr. Sci.* 446 (2013) 19–25.
- [44] L.M. Robeson, The upper bound revisited, *J. Membr. Sci.* 320 (2008) 390–400.
- [45] S. Battersby, S. Smart, B. Ladewig, S. Liu, M.C. Duke, V. Rudolph, J.C.D.D. Costa, Hydrothermal stability of cobalt silica membranes in a water gas shift membrane reactor, *Separ. Purif. Technol.* 66 (2009) 299–305.
- [46] N. Moriyama, H. Nagasawa, M. Kanezashi, K. Ito, T. Tsuru, Bis(triethoxysilyl) ethane (BTESE)-derived silica membranes: pore formation mechanism and gas permeation properties, *J. Sol. Gel Sci. Technol.* 86 (2018) 63–72.
- [47] H.F. Qureshi, R. Besselink, J.E.T. Elshof, A. Nijmeijer, L. Winnubst, Doped microporous hybrid silica membranes for gas separation, *J. Sol. Gel Sci. Technol.* 75 (2015) 180–188.
- [48] P.H.T. Ngamou, M.E. Ivanova, C. Herwartz, N. Lühmann, A. Besmehn, W. A. Meulenbergh, J. Mayer, O. Guillon, Tailoring the structure and gas permeation properties of silica membranes via binary metal oxides doping, *RSC Adv.* 5 (2015) 82717–82725.